JOURNAL OF AIRCRAFT
Vol. 49, No. 2, March–April 2012

Wind-Tunnel Balance Characterization for Hypersonic Research Applications

Keith C. Lynn,* Sean A. Commo,* and Peter A. Parker†
NASA Langley Research Center, Hampton, Virginia 23681

DOI: 10.2514/1.C031567

Wind-tunnel research was recently conducted at the NASA Langley Research Center's 31-Inch Mach 10 Hypersonic Facility in support of the Mars Science Laboratory's aerodynamic program. Researchers were interested in understanding the interaction between the freestream flow and the reaction control system onboard the entry vehicle. A five-component balance, designed for hypersonic testing with pressurized flow-through capability, was used. In addition to the aerodynamic forces, the balance was exposed to both thermal gradients and varying internal cavity pressures. Historically, the effect of these environmental conditions on the response of the balance have not been fully characterized due to the limitations in the calibration facilities. Through statistical design of experiments, thermal and pressure effects were strategically and efficiently integrated into the calibration of the balance. As a result of this new approach, researchers were able to use the balance continuously throughout the wide range of temperatures and pressures and obtain real-time results. Although this work focused on a specific application, the methodology shown can be applied more generally to any force measurement system calibration.

Nomenclature

AF	=	axial force, lb
m	=	number of whole plots
N	=	total number of runs
n	=	number of subplot runs
NF	=	normal force, lb
PM	=	pitching moment, in-lb
$\mathbf{R}$	=	correlation matrix
RM	=	rolling moment, in-lb
SF	=	side force, lb
VIF	=	variance inflation factor
$\mathbf{X}$	=	design matrix
$\mathbf{Y}$	=	matrix of responses (rNF, rPM, rRM, rYM, rSF)
YM	=	yawing moment, in-lb
$\boldsymbol{\beta}$	=	vector of regression coefficients
$\boldsymbol{\delta}$	=	whole-plot error
$\boldsymbol{\epsilon}$	=	subplot error
ρ	=	correlation of an observation
$\boldsymbol{\Sigma}$	=	variance–covariance matrix

I. Introduction

A RECENT wind-tunnel test conducted at the NASA Langley Research Center (LaRC) 31-Inch Mach 10 facility used the SS-12 balance to measure the aerodynamic loads on a scale model of the Mars Science Laboratory (MSL) aeroshell. Researchers were interested in the interaction between the onboard reaction control system (RCS) exit flow and the freestream flow. During entry into the Mars atmosphere, the RCS will be used to control both the rate damping and guidance maneuvers of the entry vehicle [1,2]. When the RCS jets are fired, the exit flow is released into a complex wake of the vehicle. Researchers suspect the interaction between the flows to have adverse effects on the aerodynamics of the aeroshell. Therefore, it is critical that these effects are fully understood and characterized. The series of wind-tunnel tests performed at the 31-Inch Mach 10 facility employed a test matrix that was designed to explore the interaction between the RCS exit flow and the wake of the vehicle over the hypersonic regime of flight.

The SS-12 is a flow-through-type balance, which allows a pressurized gas to be routed through the center of the balance and out through the model to the RCS nozzles. The experimental setup for the wind-tunnel model and the balance is shown in Fig. 1. An initial series of tests at the Mach 10 facility were conducted to obtain force and moment data for a similar model configuration when two anomalies with the SS-12 balance were discovered.

The first issue regarded an electrical zero offset reading in the side-force (SF) and yawing-moment (YM) balance outputs. These electrical zero shifts were uncovered after repeated injections of the test configuration into the freestream flow. The shift could be attributed to one or both of the following: 1) delamination of the strain gauges due to dynamic overloading of the balance and 2) deformation of the measurement beams due to dynamic overloading of the balance.

In addition to the electrical shift, there was a temperature-dependent drift in the response of the balance strain-gauge outputs over the course of a 120 s tunnel run. The force and moment measurement data drifted as the temperature of the balance increased from the nominal operating temperature at 70°F. Several different diagnostic tests were performed to evaluate the magnitude of the thermal effects. One diagnostic test in particular examined the drift behavior while the model was subject to specified RCS jet firing sequences. During a run, approximately four pressure cycles were completed, where the specified RCS jets were cycled on and off. While these cycles were executed, both the forward and aft thermocouple outputs, as well as the resulting force and moment responses on the balance output, were measured. Figure 2 shows that both the forward and aft balance temperatures increased from 70°F to approximately 112°F over the 120 s test period. Additionally, as the pressure to the RCS jets was cycled, the temperature of the balance increased, which caused a negative drift in the measurement outputs.

It was evident, as shown in Fig. 2, that the balance exhibited some nonideal behaviors, which resulted in poor data quality from the initial series of tests. The temperature drift issues were significant enough that the researchers were not confident in the data that was collected. Test engineers and researchers were forced to reevaluate the test setup, along with the overall design and calibration techniques, used for the characterization of the balance.

The following sections detail the original design of the SS-12 balance and modifications made to mitigate some of the issues

Presented as Paper 2011-950 at the 49th AIAA Aerospace Sciences Meeting, Orlando, FL, 4–7 January 2011; received 26 June 2011; revision received 11 September 2011; accepted for publication 10 October 2011.

*Research Engineer, Aeronautics Systems Engineering Branch, Mail Stop 238. Member AIAA.

†Research Engineer, Aeronautics Systems Engineering Branch, Mail Stop 238. Senior Member AIAA.

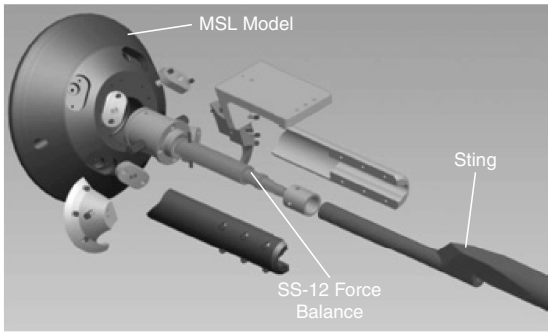

Fig. 1 31-Inch Mach 10 configuration with MSL test model.

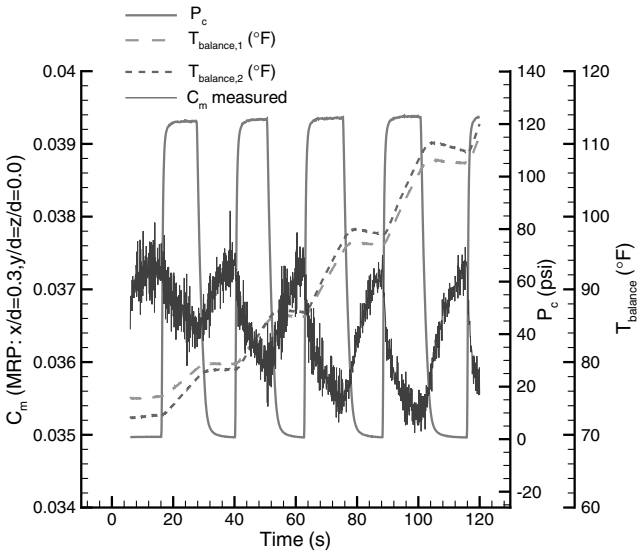

Fig. 2 Pitching-moment coefficient.

observed during the initial wind-tunnel test. Additionally, a new approach to balance calibration when subjected to environmental effects is presented. The primary focus is the methodology for the calibration design, which is generally applicable to any force measurement system.

II. Balance Calibration and Design

A. Balance Basics

The fundamental instrument that is used to directly measure the aerodynamic loads on a wind-tunnel model is known as a balance. To adequately determine these performance characteristics, it is crucial that a measurement device be used during the wind-tunnel test that is capable of accurately and precisely measuring the aerodynamic loads imparted on the test model. The balance is a transducer that is capable of providing high-precision measurements of forces and moments in up to 6 degrees of freedom.

The most critical portion of the balance development is the characterization of the balance. The purpose is to develop a mathematical model that characterizes the performance of the balance. In return, this mathematical model can be used to estimate the aerodynamic loads imparted on the model during the wind-tunnel test. When characterizing a balance, a set of predetermined calibration loads is applied to the balance, and the electrical output response of each measurement bridge is recorded. The range of the calibration loads applied to the balance during the calibration process defines the design space. Historically, the load schedule used during a calibration has been standardized based on the type of balance and calibration hardware. Specific load combinations are applied during the calibration in order to support the desired mathematical model. For example, at NASA LaRC, a second-order Taylor series expansion is used to approximate the true behavior of a balance. A

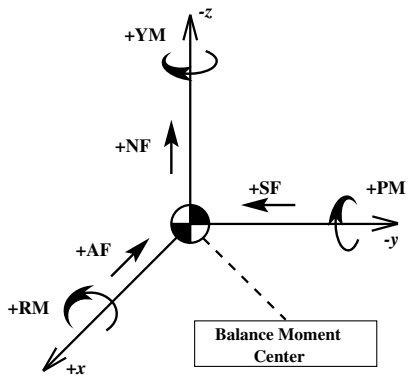

Fig. 3 Balance coordinate system.

standard six-component calibration model would contain six linear, 15 two-factor, and six pure quadratic terms. The standard balance coordinate system shown in Fig. 3 is used to define the applied loads and moments. In general, the second-order Taylor series expansion used to develop the mathematical model is

$$y = \beta_0 + \sum_{i=1}^{k} \beta_i x_i + \sum_{i=1}^{k-1} \sum_{j=i+1}^{k} \beta_{ij} x_i x_j + \sum_{i=1}^{k} \beta_{ii} x_i^2 \qquad (1)$$

where k is the number of independent variables, x_i is the ith independent variable, and β's are the regression coefficients. Based on Eq. (1),

$$1 + 2k + \frac{k(k-1)}{2}$$

calibration points are required, with at least three unique levels of each independent variable to estimate the model terms. From the regression, the calibration coefficients are delivered to the researchers at the wind tunnel in order to estimate the aerodynamic forces and moments on the test article.

When characterizing any balance, it is critical to perform a sufficient number of unique calibration loads such that all the model terms can be independently estimated. Each term in the mathematical model represents certain physical properties of the balance. The linear first-order interactions can be attributed to machining errors, errors in both location and alignment of strain gauges, and variations in the gauge factor for the strain gauges. The first-order interaction terms are typically associated with the magnitude of the deflections present during loading of the balance [3]. Typical balance calibrations have been conducted with only applied loads as being the calibration factors, but it is possible to include additional factors, such as pressure and temperature, within the calibration design if it is suspected that they have an effect on the response(s).

B. SS-12 Balance Design

The SS-12 balance is a monolithic, five-component, water-cooled, flow-through balance that measures NF, PM, RM, YM, and SF, as shown in Fig. 4. The balance was originally designed and instrumented to be a direct-read balance, which resolves the forces and moments directly, and it was instrumented to be parallel wired with a common voltage excitation input for all five components. Table 1 shows the full-scale design loads for the balance.

By using a flow-through balance, high-pressure gas can be supplied to the wind-tunnel model to simulate RCS jet firing. Instead of using a pressure bellows configuration to route the high-pressure gas to the model, the gas is routed through an internal cavity in the sting and through the balance. The gas is then routed through the internal passageways in the model out to the RCS nozzles. This particular balance was designed for testing at hypersonic facilities, which typically involves high temperatures being induced on the balance due to the heat transfer from the speed of the freestream flow over the exterior surface of the model. The balance was designed with an active cooling shield, which provides cooling to the measurement

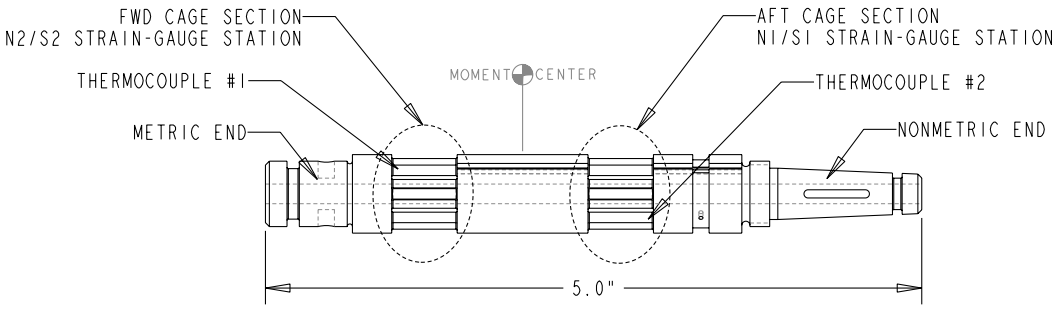

Fig. 4 SS-12 balance overview.

beams by continuously circulating cold water around the external surface of the balance, with the goal of stabilizing the temperature during testing.

During the first entry of the MSL model into the 31-Inch Mach 10 facility, the high-temperature air flowing over the model interacted with the aft sting and the heat transferred to the sting caused the temperature of the nitrogen inside the sting to increase. Whereas the aft (nonmetric) end of the balance was heated rapidly due the heated nitrogen flowing through it, the forward (metric) end of the balance was cooled by the cold water being circulated through the cooling tube jacket. The two extreme temperatures at the opposite ends of the balance resulted in large temperature gradients over the length of the balance during the 120 s runs. The presence of these large temperature gradients within the measurement sections of the balance caused the strain gauges to see large thermally induced strains, which were misinterpreted as aerodynamic loads being imparted onto the balance. Therefore, the resulting aerodynamic load measurements being recorded by the balance during the test had high errors.

These large temperature gradients resulted in repeatability issues with the measurement performance of the balance. After the initial wind-tunnel test, it was decided to reinstrument the balance with new strain gauges, and the bridge configuration was changed from the standard direct-read configuration to the standard balance (N1/N2, S1/S2, RM) configuration. With this new bridge configuration the individual strain gauges that make up a Wheatstone bridge are located at a single axial location, which reduces the sensitivity of the output responses due to thermal effects. Along with the modified balance strain-gauge layout, the mechanical setup for the MSL test setup was modified to include a shroud around aft sting with the goal of decreasing the magnitude of the temperature gradient along the length of the balance during testing. The mixture of these two modifications allowed for recharacterizing the performance of the balance, with the assumptions that performing the calibration while holding the balance at constant temperature would be representative of the expected test conditions and that temperature gradients would not need to be considered.

C. Balance Calibration Techniques

There are primarily three different types of calibration systems used today: automated calibration machines, manual calibration stands, and the single-vector system (SVS) [4,5]. Each system employs a different load schedule based upon the capabilities of the respective hardware. Using mechanically applied loads, automated machines have the ability of collecting vast amounts of data in very little time. Accordingly, the experimental designs, or load schedules, for this system are typically quite large, on the order of 1000 calibration loads. Manual test stand systems are similar to automated machines except that gravity based loads, or deadweights, are used instead of mechanically applied loads. Manual stand systems apply on the same order of runs as an automated machine but require considerably more time, due to the calibration hardware.

Table 1 SS-12 balance design loads

	Design load	
Component	English units	Metric units
NF	100 lb	444.8 N
AF	N/A	N/A
PM	150 in-lb	16.9 N-m
RM	32 in-lb	3.6 N-m
YM	40 in-lb	4.5 N-m
SF	30 lb	133.4 N

Both the automated and manual stand systems were designed around the one-factor-at-a-time (OFAT) calibration design methodology. Weaknesses of this approach have led engineers to develop experimental designs sweeping two factors simultaneously, necessary to calculate interaction coefficients of the mathematical model [6]. Although the calibration loads applied during both automated and manual systems are based on the OFAT principles, there are certain load combinations that are applied that allow for computing the nonlinear and quadratic coefficients necessary for the desired mathematical model. Without using a rigorously statistical approach, the experimental designs created for the manual and automated systems contain a vast number of runs that exhaust all combinations of two-component loads. The costs associated with executing these designs are further increased when including other factors, such as pressure and temperature, in the calibration. Fully crossing pressure and temperature with these experimental designs can more than quadruple the required number of runs, which could take months to complete using a manual test stand system.

The SVS uses a single deadweight load to apply up to six loads simultaneously by changing the orientation of the balance relative to gravity. As the balance orientation relative to gravity changes, the applied load vector results in varying the magnitudes of the applied loads on the balance. The load schedule for the SVS is based on a popular class of response surface designs known as a central composite design (CCD) [7,8]. Originally developed in 1951 by Box and Wilson for chemical processes, CCDs are used frequently in experiments where the response is approximated by a second-order function. They augmented a standard first-order, or factorial, design with axial, or star, points to estimate the second-order effects in the mathematical model. For experiments with a large number of independent variables, a fraction of the full factorial can be used. The SVS employs a 2^{6-1} fractional factorial for a standard six-component balance, but it is slightly modified to accommodate the physics-based constraint of the SVS, which is discussed later. The factorial portion of the load schedule consists of 37 runs where all six components are loaded simultaneously. The axial portion consists of 27 runs that loads one or two components at a time. A 28-term second-order model is estimated using these 64 runs. The relatively low number of runs used by the SVS makes it a suitable method for calibrating at temperature and pressure.

D. Balance Calibration Experimental Design

For calibration applications, the limitations of the calibration apparatus cannot be ignored when developing an experimental design. The most important phase of an experiment is the preexperimental planning, where the goals, response variables, and input factors of the experiment are established. Based on the objectives and possible outcomes of an experiment, a successful approach can be formulated. In general, most balance character-

Table 2 Calibration response variables

Response	Response, units	Nomenclature
1	Normal-force bridge output, mV/V	rNF
2	Pitching-moment bridge output, mV/V	rPM
3	Rolling-moment bridge output, mV/V	rRM
4	Yawing-moment bridge output, mV/V	rYM
5	Side-force bridge output, mV/V	rSF

ization applications use response surface methods, either explicitly or implicitly, where the calibration system is reasonably well-understood and delivering a mathematical calibration model is required. However, in instances where no previous system knowledge is available, a preliminary, factor-screening experiment can be conducted to eliminate unimportant factors before the comprehensive characterization experiment. This approach is known as sequential experimentation and is a strategic and rigorous approach often used in experimental design [8,9].

The response variables are the parameters that are measured during an experiment. In balance calibration, the response variables are the strain-gauge outputs and are shown in Table 2. The input factors can be divided into four types: controlled design factors, held-constant factors, uncontrolled factors, and nuisance factors. Controlled design factors are varied during the experiment over specified ranges to study their effects on the response variables. The controlled design factors for this calibration are shown in Table 3. Held-constant and uncontrolled factors are not studied during an experiment, because the effects on the responses due to these factors are small and assumed to be negligible. Nuisance factors can be controlled or uncontrolled but their effect on the responses may not be small. Although these nuisance factors may not be of interest, it should be recognized that they are present, and precautions should be taken to limit their effect. Blocking is a useful technique in limiting the effect of nuisance factors [8,9].

When designing an experiment, three concepts are emphasized: randomization, replication, and blocking [9]. Randomization defends against systematic errors in an experiment. Because the runs are executed randomly, any effects due to hysteresis, or other systematic behaviors, are minimized. Replication provides information about the pure experimental error of the response variables. For a given set of factor combinations that is replicated t times, then there are $t-1$ degrees of freedom available to estimate the repeatability, which is an important statistic in any calibration. Finally, as mentioned earlier, blocking is a preventative technique that is used to minimize the effect of any lurking variables in the experiment. Blocks are organized such that orthogonality of the factors is retained in the design matrix. Orthogonality, from the regression perspective, ensures linear independence between terms in the mathematical model. The current SVS calibrations incorporate a randomized block design, which is a near-orthogonal design.

Characterizing the SS-12 balance to meet the objectives of the researchers posed two new challenges. First, since there were no strain gauges to measure axial force, a reduced version of the standard SVS calibration design was developed and employed. The reduced, five-component design, shown in Table 4, contained 42 design points as compared with the six-component design, which contains 64 design points. Second, the average balance temperature and internal cavity pressure were suspected to effect the strain-gauge responses and were integrated into the design of the calibration. Historically, only single-component loads were performed at the expected wind-tunnel operating conditions during calibration, and only adjustments of the primary sensitivities during data reduction at the wind tunnel were performed. However, it was decided to model the balance outputs as a continuous function of the environmental variables, temperature and pressure, instead of at discrete points. Designing an efficient yet robust calibration to include these new independent variables was critical.

Table 4 Five-component SVS calibration design[a]

NF	PM	RM	YM	SF
	Fractional factorial			
−48	−72	±15	−19	−13
−48	−72	±15	19	13
−48	72	±15	−19	13
−48	72	±15	19	−13
48	−72	±15	19	−13
48	−72	±15	−19	13
0	0	0	0	0
	Axial			
±100	0	0	0	0
±100	±150	0	0	0
±100	0	0	0	±30
±100	0	±32	0	0
0	0	0	±40	±30
0	0	0	0	±30
0	0	0	0	0

[a]Note that all load combinations within the table represent vectors.

The SS-12 characterization experiment used restricted randomization since changing temperature was more time consuming than changing pressure or the applied forces and moments. In the NASA LaRC force measurement laboratory, approximately 2 h were required for the balance temperature to stabilize while the pressure and applied forces and moments were set within a minute. To accommodate this practical execution restriction, the balance temperature was set and held constant, while the other six factors were varied randomly. This type of experimental design is known as a split-plot design (SPD). The ideology and concepts of a SPD are attributed to their application in agricultural experiments [10]. Hard-to-change factors were applied over large plots of land and were conveniently called whole plots. The easy-to-change factors were crops (and other variables) within a large plot of land and became known as subplots. Temperature was the only whole-plot factor in the calibration while the other factors were subplot factors. By design, every whole plot in the calibration contained the same subplot design, which is known as a crossed design. These types of SPDs have convenient statistical properties, such as equivalent estimation. However, with any SPD, the error structure must be considered in the analysis [11–13].

The general form of the mathematical model for a SPD can be written as

$$\mathbf{y} = \mathbf{X}\boldsymbol{\beta} + \boldsymbol{\delta} + \boldsymbol{\epsilon} \tag{2}$$

where $\mathbf{y}$ is a $N \times 1$ vector of responses, $\mathbf{X}$ is a $N \times p$ model matrix, $\boldsymbol{\beta}$ is a $p \times 1$ vector of regression coefficients, $\boldsymbol{\delta}$ is a $N \times 1$ vector of

Table 3 Calibration design factors

Factor label	Design factor	Nomenclature	Range	
			English units	Metric units
1 ($x1$)	Average balance temperature	T	70 to 120°F	21 to 49°C
2 ($x2$)	Balance cavity pressure	P	14.7 to 400 psia	101.4 to 2758 kPa
3 ($x3$)	Normal force	NF	−100 to 100 lb	−444.8 to 444.8 N
4 ($x4$)	Pitching moment	PM	−150 to 150 in-lb	−16.9 to 16.9 N-m
5 ($x5$)	Rolling moment	RM	−32 to 32 in-lb	−3.6 to 3.6 N-m
6 ($x6$)	Yawing moment	YM	−40 to 40 in-lb	−4.5 to 4.5 N-m
7 ($x7$)	Side force	SF	−30 to 30 lb	−133.4 to 133.4 N

random whole-plot errors, $\boldsymbol{\epsilon}$ is a $N \times 1$ vector of random subplot errors, N is the total number of runs, and p is the total number of terms in the model including the intercept. Equation (2) is a more flexible form of the typical linear model $\mathbf{y} = \mathbf{X}\boldsymbol{\beta} + \boldsymbol{\epsilon}$ as it permits correlation and nonhomogeneous variances. It is assumed that $\boldsymbol{\delta} + \boldsymbol{\epsilon}$ has a mean of $\mathbf{0}$ and a variance–covariance matrix of

$$\boldsymbol{\Sigma} = \sigma_\epsilon^2 \mathbf{I} + \sigma_\delta^2 \mathbf{J}_b \tag{3}$$

where $\mathbf{I}$ is an identity matrix of size N, σ_ϵ^2 is the subplot error variance, and σ_δ^2 is the whole-plot error variance. Since the experimental design is completely crossed,

$$\mathbf{J}_b = \mathbf{I}_m \otimes \mathbf{J}_n \tag{4}$$

where m is the number of whole plots, n is the number of subplot runs within a whole plot, and $\mathbf{J}_n$ is a $n \times n$ matrix of ones. The matrix $\mathbf{J}_b$ has the form

$$\mathbf{J}_b = \begin{bmatrix} \mathbf{1}_n\mathbf{1}_n' & \mathbf{0} & \dots & \mathbf{0} \\ \mathbf{0} & \mathbf{1}_n\mathbf{1}_n' & \dots & \mathbf{0} \\ \vdots & \vdots & \ddots & \vdots \\ \mathbf{0} & \mathbf{0} & \dots & \mathbf{1}_n\mathbf{1}_n' \end{bmatrix} \tag{5}$$

The correlation of an individual observation is expressed as

$$\rho = \frac{\sigma_\delta^2}{\sigma_\epsilon^2 + \sigma_\delta^2} \tag{6}$$

The correlation matrix of the observations is a block diagonal matrix of the form

$$\frac{1}{\sigma_\epsilon^2 + \sigma_\delta^2}\boldsymbol{\Sigma} = \mathbf{R} = \begin{bmatrix} 1 & \rho & \dots & \rho & & & & & & & & \\ \rho & 1 & \dots & \rho & & & \mathbf{0} & & \dots & & \mathbf{0} & \\ \vdots & \vdots & \ddots & \vdots & & & & & & & & \\ \rho & \rho & \dots & 1 & & & & & & & & \\ & & & & 1 & \rho & \dots & \rho & & & & \\ & & & & \rho & 1 & \dots & \rho & & & & \\ & \mathbf{0} & & & \vdots & \vdots & \ddots & \vdots & \dots & & \mathbf{0} & \\ & & & & \rho & \rho & \dots & 1 & & & & \\ & \vdots & & & & \vdots & & & \ddots & & \vdots & \\ & & & & & & & & & 1 & \rho & \dots & \rho \\ & & & & & & & & & \rho & 1 & \dots & \rho \\ & \mathbf{0} & & & & \mathbf{0} & & & \dots & \vdots & \vdots & \ddots & \vdots \\ & & & & & & & & & \rho & \rho & \dots & 1 \end{bmatrix} \tag{7}$$

From the correlation matrix in Eq. (7), it can be seen that observations in different whole plots are independent, while observations within a whole plot are correlated, since the offdiagonal elements are nonzero within a block. In terms of the SS-12 calibration, there was a degree of correlation between observations as a result of having to hold the temperature constant during each whole plot.

Because of the correlation among the observations due to the restricted randomization, the ordinary least-squares estimator of $\boldsymbol{\beta}$ is not the most appropriate method since it does not consider the variance–covariance matrix $\boldsymbol{\Sigma}$. Instead, generalized least squares (GLS) can be used, which minimizes $(\mathbf{y} - \mathbf{X}\boldsymbol{\beta})'\boldsymbol{\Sigma}^{-1}(\mathbf{y} - \mathbf{X}\boldsymbol{\beta})$. The best linear unbiased estimator (BLUE) of $\boldsymbol{\beta}$ is

$$\hat{\boldsymbol{\beta}} = (\mathbf{X}'\boldsymbol{\Sigma}^{-1}\mathbf{X})^{-1}\mathbf{X}'\boldsymbol{\Sigma}^{-1}\mathbf{y} \tag{8}$$

with the variance of the estimates given by $\text{var}(\hat{\boldsymbol{\beta}}) = (\mathbf{X}'\boldsymbol{\Sigma}^{-1}\mathbf{X})^{-1}$. However, since $\boldsymbol{\Sigma}$ is unknown, the estimate is no longer the BLUE. Therefore,

$$\hat{\boldsymbol{\beta}} = (\mathbf{X}'\hat{\boldsymbol{\Sigma}}^{-1}\mathbf{X})^{-1}\mathbf{X}'\hat{\boldsymbol{\Sigma}}^{-1}\mathbf{y} \tag{9}$$

where $\hat{\sigma}_\epsilon^2$ and $\hat{\sigma}_\delta^2$ are estimates of the true, unknown variances σ_ϵ^2 and σ_δ^2, respectively, and are used to construct $\hat{\boldsymbol{\Sigma}}$. The method of maximum likelihood is one approach to obtain the variance estimates. Based on the general model form given in Eq. (2), the likelihood function can be divided in to two parts: one containing the fixed effects $\mathbf{X}\boldsymbol{\beta}$ and one containing the random effects $\boldsymbol{\delta}$ and $\boldsymbol{\epsilon}$. This separation of fixed and random effects results in a mixed model [14,15]. Restricted maximum likelihood (REML) estimators of the variance components are obtained from the random part of the model and are then substituted into the known form of the covariance matrix in Eq. (3). Using Eq. (9), the GLS estimators are obtained. However, REML does not require an experimental design to be crossed or balanced (equally sized whole plots).

The newly developed experimental design for SS-12 is shown in Table 5. Although it is not representative (does not include all runs, not randomized) of the exact run order, Table 5 reveals how temperature and pressure were integrated in to the reduced five-component SVS design. Table 5 shows all the factor combinations that were conducted during the calibration. The entire experimental design required eight days to complete the 1028 runs and is shown in Table 6. The first two days of the calibration were conducted at ambient temperature and pressure to ensure the balance and related calibration system were operating as expected. Each day consisted of one block in the design accompanied by a tare sequence performed at the beginning and end of the day. For each tare sequence, five tare models were constructed for each level of pressure and temperature, which describes the nominal response of each bridge as a function of balance orientation. The tare models were implemented such that at a given temperature and pressure, the appropriate tare model was applied in the data reduction. The calculated tare loads were then added to the applied loads, resulting in a true load that was finally used to develop the models.

Based on the calibration design matrix, the supported 35-term calibration model for one strain gauge is

$$y = \beta_0 + \sum_{i=1}^{7}\beta_i x_i + \sum_{i=1}^{6}\sum_{j=i+1}^{7}\beta_{ij}x_i x_j + \sum_{i=2}^{7}\beta_{ii}x_i^2 \tag{10}$$

It can be seen that the strain-gauge output y is a function of temperature, pressure, and applied forces and moments. It should be noted that in the above equation the quadratic temperature term T^2 (x_1^2) is not included. Five calibration models are developed for the five output responses, resulting in a 35×5 matrix of regression coefficients. The model is an augmentation of the standard second-order model given in Eq. (1). It was formulated under the assumption that temperature has primarily a linear effect on the response of each measurement component, which is based on the experience of balance engineers and previous experiments conducted to obtain temperature corrections. Accordingly, only two unique temperature levels were required.

E. Physical Constraints of the SVS

The SVS calibration methodology is based on applying a single load vector to the balance, where a system of forces and moments are reduced to a single resultant force vector acting at a point. For this to occur, the system of applied forces and moments must be able to be reduced such that the resultant force and moment vectors are mutually perpendicular to each other. In doing so, an infinite number of possible load combinations can be applied to a balance during calibration, but an arbitrary combination of both forces and moments cannot be applied. This limitation on arbitrary load combinations is a physical constraint of the SVS system. The perpendicular relationship that exists between resultant force and moment vectors is expressed as the dot product between the two vectors, and by setting the cosine of the angle between the two equal to zero, the resulting relationship is established (for a six-component balance) [5]:

Table 5 SS-12 balance calibration design (in English units)[a]

NF	PM	RM	YM	SF
Whole plot 1, T = 70, P = 14.7				
−48	−72	±15	−19	−13
−48	−72	±15	19	13
−48	72	±15	−19	13
−48	72	±15	19	−13
48	−72	±15	19	−13
48	−72	±15	−19	13
±100	0	0	0	0
±100	±150	0	0	0
±100	0	0	0	±30
±100	0	±32	0	0
0	0	0	±40	±30
0	0	0	0	±30
0	0	0	0	0
Whole plot 2, T = 120, P = 14.7, 120, 200, 400				
−48	−72	±15	−19	−13
−48	−72	±15	19	13
−48	72	±15	−19	13
−48	72	±15	19	−13
48	−72	±15	19	−13
48	−72	±15	−19	13
±100	0	0	0	0
±100	±150	0	0	0
±100	0	0	0	±30
±100	0	±32	0	0
0	0	0	±40	±30
0	0	0	0	±30
0	0	0	0	0
Whole plot 3, T = 70, P = 14.7, 120, 200, 400				
−48	−72	±15	−19	−13
−48	−72	±15	19	13
−48	−72	±15	−19	13
−48	72	±15	19	−13
48	−72	±15	19	−13
48	−72	±15	−19	13
±100	0	0	0	0
±100	±150	0	0	0
±100	0	0	0	±30
±100	0	±32	0	0
0	0	0	±40	±30
0	0	0	0	±30
0	0	0	0	0
Whole plot 4, T = 120, P = 14.7, 120, 200, 400				
−48	−72	±15	−19	−13
−48	−72	±15	19	13
−48	72	±15	19	−13
−48	72	±15	19	−13
48	−72	±15	19	−13
48	−72	±15	−19	13
±100	0	0	0	0
±100	±150	0	0	0
±100	0	0	0	±30
±100	0	±32	0	0
0	0	0	±40	±30
0	0	0	0	±30
0	0	0	0	0

[a]Note that all load combinations within the table represent vectors.

Table 7 VIF of calibration model terms

Model term	VIF
Linear	
x_1 (temp.)	6.8756
x_2 (pressure)	5.5404
x_3 (NF)	2.5604
x_4 (PM)	2.5488
x_5 (RM)	2.5306
x_6 (YM)	2.4310
x_7 (SF)	2.4554
Two-factor interactions	
x_1x_2	1.2352
x_1x_3	1.1280
x_1x_4	1.1936
x_1x_5	1.1592
x_1x_6	1.0806
x_1x_7	1.1417
x_2x_3	1.2025
x_2x_4	1.3300
x_2x_5	1.1997
x_2x_6	1.1049
x_2x_7	1.2105
x_3x_4	1.0284
x_3x_5	1.0390
x_3x_6	1.1063
x_3x_7	1.4104
x_4x_5	1.0000
x_4x_6	1.4656
x_5x_6	1.0000
x_5x_7	1.0411
x_6x_7	1.0347
Pure quadratics	
x_2^2	1.1838
x_3^2	4.1466
x_4^2	2.8474
x_5^2	2.7276
x_6^2	2.5074
x_7^2	3.3055

$$\frac{-(\mathrm{RM})(\mathrm{AF}) + (\mathrm{PM})(\mathrm{SF}) - (\mathrm{YM})(\mathrm{NF})}{(\sqrt{\mathrm{RM}^2 + \mathrm{PM}^2 + \mathrm{YM}^2})(\sqrt{\mathrm{AF}^2 + \mathrm{SF}^2 + \mathrm{NF}^2})} = 0 \qquad (11)$$

The governing equation that constrains the relative direction and magnitude of each of the applied load components using a single load vector is

$$-(\mathrm{RM})(\mathrm{AF}) + (\mathrm{PM})(\mathrm{SF}) - (\mathrm{YM})(\mathrm{NF}) = 0 \qquad (12)$$

This physical constraint of the SVS signifies three possible load combinations that cannot be independently applied during a balance calibration: RM/AF, PM/SF, and YM/NF. Therefore, there exists no possible combination of force and moment vectors that can be applied during an SVS calibration that result in a load point where only RM/AF, PM/SF, or YM/NF are applied. Because this constraint within the SVS exists, multicollinearity exists between these three interaction terms within the calibration model. For the calibration of the SS-12 balance, the RM/AF constraint does not exist since the balance does not have an AF component. Although one of the interaction terms disappears, the remaining interaction terms still cannot be estimated orthogonally. As a result, one of the remaining

Table 6 Execution of the experimental design

	Original		Modified						
	Day 1	Day 2	Day 3	Day 4	Day 5	Day 6	Day 7	Day 8	Total
Tare runs	36	24	96	96	96	96	96	96	636
Calibration runs	42	0	46	41	45	43	45	43	305
Confirmation runs	0	20	12	11	11	11	11	11	87
Total runs	78	44	154	148	152	150	152	150	1028
Temperature, °F	77	77	120	120	77	77	120	120	-
Pressure levels	1	1	4	4	4	4	4	4	-

terms is neglected in the regression modeling to eliminate any multicollinearity issues.

F. Properties of the Experimental Design

When developing the experimental design for characterizing the SS-12 balance, several important features were incorporated. These experimental design features were directly related to addressing the specific experimental objectives. Some of the features included in the SS-12 design were 1) sufficient number of data points throughout the calibration design space, 2) orthogonal blocking, 3) precise model coefficient estimates, 4) favorable prediction variance over calibration design space, 5) robust calibration, and 6) execution efficiency [9].

As with any experimental design, the quality of the SS-12 experimental design was evaluated before executing the calibration. The variance inflation factor (VIF) is one metric for assessing the quality of the experimental design. It is a measure of the multicollinearity, or linear dependency, in the regressor variables. The VIF is calculated as

$$\mathrm{VIF}\,(\hat{\boldsymbol{\beta}}) = \mathrm{diag}[(\mathbf{R}'\mathbf{R})^{-1}] \tag{13}$$

where $\mathbf{R}$ is the correlation matrix for the design [16]. For complete orthogonality, $(\mathbf{R}'\mathbf{R}) = \mathbf{I}$. It is a generally accepted in the balance community to set the upper limit of 5–10 on the VIF [17,18]. The presence of multicollinearity within a linear regression directly impacts the precision with which regression coefficients can be estimated, so any values of VIF greater than 10 indicates possible flaws within the experimental design. Table 7 lists the VIF values for the experimental design for the SS-12 balance calibration.

The standard error of prediction, or prediction variance, is a computed value that provides a estimate on the quality of the predicted responses, based entirely on the experimental design. Given a particular experimental design, the prediction variance is calculated as

$$\mathrm{Var}\,[\hat{\mathbf{y}}(\mathbf{x}_0)] = \sigma^2(\mathbf{x}_0'(\mathbf{X}'\mathbf{X})^{-1}\mathbf{x}_0) \tag{14}$$

where $\mathbf{x}_0$ represents the location of a point within the design space. Essentially, the variance is a scale factor for the prediction variance. For a SPD, Eq. (14) becomes

$$\mathrm{Var}\,[\hat{\mathbf{y}}(\mathbf{x}_0)] = \mathbf{x}_0'(\mathbf{X}'\boldsymbol{\Sigma}^{-1}\mathbf{X})^{-1}\mathbf{x}_0 \tag{15}$$

For a CCD, the computed values are especially sensitive to the location of the axial (single-loaded) points within the design space, as well as the quantity of center runs that are executed [19]. Response surface plots are an efficient method to check the prediction variance

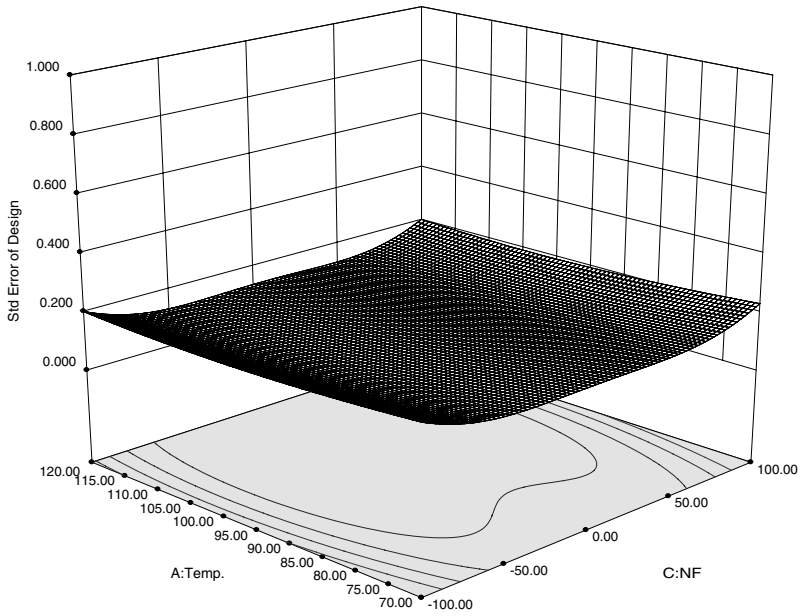

Fig. 5 Typical prediction variance profile.

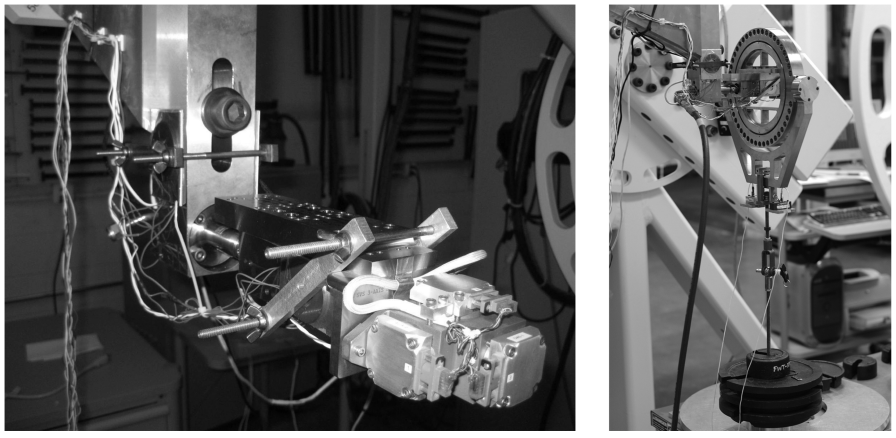

a) Balance (inside fixture) mounted in SVS stand and 3-axis accelerometer package

b) Rear view showing pressure lines and applied dead-weights

Fig. 6 SS-12 SVS calibration setup.

Table 8 Full-scale outputs and linear sensitivities

	rNF	rPM	rRM	rYM	rSF
Full-scale output, mV/V	2.650	2.959	0.701	3.534	1.990
Linear sensitivity, lb/(mV/V) or in-lb/(mV/V)	37.742	50.685	45.681	11.317	15.077
Linear sensitivity, N/(mV/V) or N-m/(mV/V)	167.889	5.727	5.162	1.279	67.066

of a design. Ideally, the surface should be flat, which signifies constant prediction properties across the entire design space. Figure 5 is an example of a typical prediction variance profile.

III. Calibration Setup and Execution

The hardware and experimental setup for the calibration of the SS-12 balance is shown in Fig. 6. The balance is installed inside of its balance calibration block, and the SVS template is installed onto the balance calibration block. The balance calibration block has a specially designed cap plate that mounts to its forward most end, which caps off the balance and calibration block allowing the system to be statically pressurized up to 600 psia. This assembly was then mounted to the SVS backstop, which is attached to a set of motors that allow the balance to both pitch and roll to any specified set of angles, allowing the balance to be positioned at any position in space. To calibrate the balance at specific pressures and temperatures, the standard SVS calibration configuration was modified to accept these new calibration features.

To apply constant static pressures to the internal cavity of the balance, the taper adapter that was used to mount the balance to the SVS backstop was modified to add a through hole with a tapped hole at its aft end to accommodate a pressure fitting. A bottle of compressed nitrogen was connected to the taper adapter, and a digital pressure gauge was placed in line between the bottle and the balance. The digital pressure gauge was wired into the data acquisition system, and the pressure measurement at each calibration load point was precisely measured to within 0.1 psia. During the calibration the applied static pressure was varied by manually adjusting a valve on the nitrogen cylinder, and the output was monitored on a digital pressure gauge.

A series of resistive-type foil heaters were attached to the balance calibration block and the backstop directly aft of where the balance mounts to the SVS allowing both the balance and the backstop to be heated to a constant temperature. These heaters were attached to an active feedback control system, which actively controlled the temperature being applied to the balance using a series of thermocouples that measured the local temperatures at the heaters. During this process, the thermocouples located in the forward and aft sections of the balance were monitored, and the heater control system was adjusted to ensure the average temperature between the forward and aft cage sections was maintained within an acceptable range ($\pm 2^{\circ}$F) of the nominal temperature setting necessary for the calibration load schedule.

IV. Data Analysis

The calibration models were developed using GLS, and the variance components were estimated using REML. However, since the experimental design was crossed, the equivalence property holds and ordinary least squares (OLS) is also appropriate for estimating the model coefficients. This is particularly powerful when REML is unavailable, but it should be noted that model reduction should not be performed under OLS since it does not consider the correlation among the observations. Using GLS in combination with REML, model reduction was performed using the backward-selection method and a cutoff criteria of 0.05. The full-scale outputs and measurement sensitivities for each bridge are shown in Table 8.

Figure 7 shows the percent of full-scale effect for terms in each of the five models, shown in decreasing order. Full-scale effects are calculated as the size of a given model coefficient relative to the primary sensitivity. Therefore, the primary sensitivities are not shown in the figure as they dominate. The absence of any significant temperature linear effects could be attributed to the thermal correcting properties of the Wheatstone bridges and/or the gauge-matching technique used at NASA LaRC [20].

From Table 9, it is evident that the effects are small compared with the primary sensitivities on each component. The linear effects, on average, are the largest group but still only account for a small percentage of the total effect for each component.

Both experimental design points and confirmations points were used to calculate the standard deviation between the applied loads and the loads calculated from the regression models. Historically, within the balance and wind-tunnel communities the standard deviation of the residuals is the standard practice used to quote the balance accuracy. The experimental design contained 305 runs, with 87 confirmation points interspersed throughout the design, which amounted to 392 total runs to estimate the standard deviation.

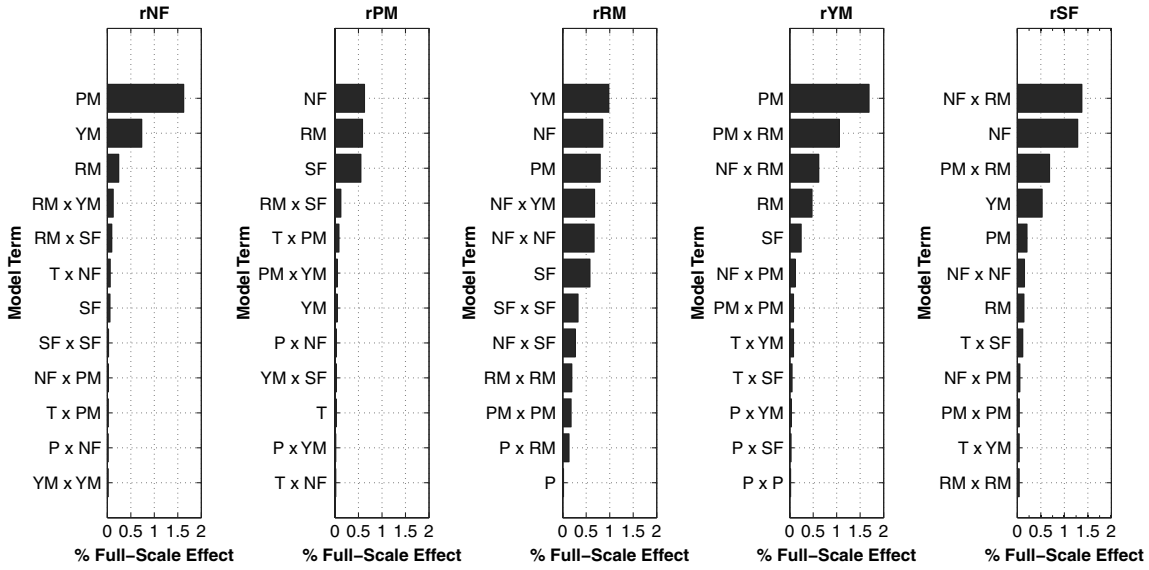

Fig. 7 Percent of full-scale effects.

Table 9 Model term contribution

	rNF	rPM	rRM	rYM	rSF
Linear, % full scale	2.66	1.81	3.22	2.43	2.16
2FI and quadratic, % full scale	0.29	0.25	2.32	1.88	2.37
Pressure and temperature, % full scale	0.12	0.18	0.15	0.24	0.18

Table 10 Accuracy of SS-12 balance responses

	rNF	rPM	rRM	rYM	rSF
Two-sigma including pressure and temperature terms, % full scale	0.085	0.078	0.477	0.151	0.162
Two-sigma excluding pressure and temperature terms, % full scale	0.117	0.114	0.484	0.175	0.202

Table 10 shows the final two-sigma accuracies, both with and without the pressure and temperature terms included in the model. The model that was used without pressure and temperature originally contained 20 terms, made up of five main effects, 10 two-factor interactions, and five quadratic terms. The 20-term model was then reduced using a backward-selection method, from which two-sigma accuracies were computed. From Table 10, it is clear that all five components have improved accuracies when pressure and temperature are included in the calibration model for each measurement component.

Upon completion of the calibration and analysis of the resulting mathematical models, the regression coefficients were provided to the wind tunnel. In addition to the regression coefficients, an algorithm was provided to the wind tunnel, which allowed for computing the resulting loads from the strain-gauge outputs. The algorithm used to compute the loads from the strain-gauge outputs is a modified version of the load calculation method described in the AIAA Recommended Practice document for internal strain-gauge balance [6]. The Appendix provides detail on the data reduction equations used to compute the loads, with emphasis on how the standard method was modified to implement the additional terms including pressure and temperature.

V. Conclusions

Typically, balance calibrations only consider the effects of applied loads on the output of the measurement bridges. However, in some research applications, like hypersonics, additional factors, such as temperature, can potentially influence the behavior of the balance during testing. Some recent work has studied how to integrate the effects of temperature and other factors into both the calibration and the use of the balance, but availability of literature in both of these areas is extremely limited.

During preliminary testing in the 31-Inch Mach 10 facility for the MSL program, temperature and pressure were observed to have an impact on the behavior of the SS-12 balance. After some redesign work, which included relocation of the measurement bridges, the balance was calibrated while considering temperature and pressure effects. Through statistical design of experiments, an efficient, robust calibration design was developed and executed. The measurement accuracies of the balance clearly improved as a result of including temperature and pressure in the calibration. Furthermore, during follow-up testing for MSL, researchers were able to obtain real-time results because the calibration models were continuous functions of temperature and pressure. Historically, single-component loads at the expected operating conditions were used to correct the primary sensitivities of the measurement bridges, and the corrections to the wind-tunnel data were done after the completion of testing.

The techniques presented here can be applied to any force measurement calibration. Although the paper discussed a specific example related to the SS-12 balance and the SVS calibration hardware, the principles used to develop the calibration design in this paper can be easily modified for other applications with different calibration hardware.

Appendix: SS-12 Balance Data Reduction Equation

The predicted response of a single strain gauge is given by

$$\begin{aligned}\hat{y}(T,\ldots,\mathrm{SF}) &= \hat{\beta}_0 + \hat{\beta}_1 T + \hat{\beta}_2 P + \hat{\beta}_3 \mathrm{NF} + \hat{\beta}_4 \mathrm{PM} + \hat{\beta}_5 \mathrm{RM} \\ &+ \hat{\beta}_6 \mathrm{YM} + \hat{\beta}_7 \mathrm{SF} + \hat{\beta}_{22} P^2 + \hat{\beta}_{33} \mathrm{NF}^2 + \hat{\beta}_{44} \mathrm{PM}^2 + \hat{\beta}_{55} \mathrm{RM}^2 \\ &+ \hat{\beta}_{66} \mathrm{YM}^2 + \hat{\beta}_{77} \mathrm{SF}^2 + \hat{\beta}_{12} T \times P + \hat{\beta}_{13} T \times \mathrm{NF} + \hat{\beta}_{14} T \\ &\times \mathrm{PM} + \hat{\beta}_{15} T \times \mathrm{RM} + \hat{\beta}_{16} T \times \mathrm{YM} + \hat{\beta}_{17} T \times \mathrm{SF} + \hat{\beta}_{23} P \\ &\times \mathrm{NF} + \hat{\beta}_{24} P \times \mathrm{PM} + \hat{\beta}_{25} P \times \mathrm{RM} + \hat{\beta}_{26} P \times \mathrm{YM} + \hat{\beta}_{27} P \\ &\times \mathrm{SF} + \hat{\beta}_{34} \mathrm{NF} \times \mathrm{PM} + \hat{\beta}_{35} \mathrm{NF} \times \mathrm{RM} + \hat{\beta}_{36} \mathrm{NF} \times \mathrm{YM} \\ &+ \hat{\beta}_{37} \mathrm{NF} \times \mathrm{SF} + \hat{\beta}_{45} \mathrm{PM} \times \mathrm{RM} + \hat{\beta}_{46} \mathrm{PM} \times \mathrm{YM} + \hat{\beta}_{47} \mathrm{PM} \\ &\times \mathrm{SF} + \hat{\beta}_{56} \mathrm{RM} \times \mathrm{YM} + \hat{\beta}_{57} \mathrm{RM} \times \mathrm{SF} + \hat{\beta}_{67} \mathrm{YM} \times \mathrm{SF}\end{aligned}$$

$$\hat{y}(\mathbf{x}_0) = \mathbf{x}_0 \underline{\hat{\boldsymbol{\beta}}} \tag{A1}$$

where $\mathbf{x}_0$ is a 1×35 expanded vector of the temperature, pressure, and applied loads, and $\underline{\hat{\boldsymbol{\beta}}}$ is a 35×1 vector of regression coefficients. For SS-12, there are five strain gauges, so Eq. (A1) becomes

$$\hat{\mathbf{y}} = \mathbf{x}_0 \hat{\boldsymbol{\beta}} \tag{A2}$$

where $\hat{\mathbf{y}}$ is a 1×5 vector of the predicted responses and $\hat{\boldsymbol{\beta}}$ is a 35×5 matrix of regression coefficients. For statistically insignificant terms, their respective elements within the regression coefficient matrix are set to zero. The terms on the right side of Eq. (A2) can be expressed as

$$\mathbf{x}_0 = [1 \vdots \mathbf{x}_0^*] \qquad \hat{\boldsymbol{\beta}} = \begin{bmatrix} \hat{\boldsymbol{\beta}}_0 \\ \cdots \\ \hat{\boldsymbol{\beta}}^* \end{bmatrix}$$

Therefore, Eq. (A2) can be written as

$$\hat{\mathbf{y}} = 1\hat{\boldsymbol{\beta}}_0 + \mathbf{x}_0^* \hat{\boldsymbol{\beta}}^* = \hat{\boldsymbol{\beta}}_0 + \mathbf{x}_0^* \hat{\boldsymbol{\beta}}^*$$

Subtracting the zero-intercept from the gauge output gives the delta bridge output, or

$$\boldsymbol{\delta}\hat{\mathbf{y}} = \hat{\mathbf{y}} - \hat{\boldsymbol{\beta}}_0 = \mathbf{x}_0^* \hat{\boldsymbol{\beta}}^* \tag{A3}$$

Equation (A3) represents the predicted responses of the strain gauges for an unloaded balance. The calibration equations in Eq. (A3) are of the form $\hat{\mathbf{y}} = f(\mathbf{x}_0)$, but during use in the wind tunnel, the loads imparted on the balance are estimated from the measured strain-gauge outputs or, more specifically, $\hat{\mathbf{x}}_0 = f(\mathbf{y})$. Because the calibration equations are second-order, an iterative scheme is used to estimate the loads. The load iteration algorithm begins by dividing $\mathbf{x}_0^*$ and $\hat{\boldsymbol{\beta}}^*$ into three parts. For standard balance calibrations without temperature and pressure, $\mathbf{x}_0^*$ and $\hat{\boldsymbol{\beta}}^*$ are divided into two parts [6]. Starting with $\mathbf{x}_0^*$,

$$\mathbf{x}_0^* \Rightarrow \left[\mathbf{x}_{0_1}^*, \mathbf{x}_{0_2}^*, \mathbf{x}_{0_3}^*\right]$$

where $\mathbf{x}_{0_1}^* = [\mathrm{NF}, \mathrm{PM}, \mathrm{RM}, \mathrm{YM}, \mathrm{SF}]$, $\mathbf{x}_{0_2}^* = [T, P, T \times P, P^2]$, and $\mathbf{x}_{0_3}^*$ is a 1×25 vector of the remaining higher-order loading combinations, including the interactions with temperature and pressure. Similarly, the coefficient matrix, $\hat{\boldsymbol{\beta}}^*$ can be partitioned as

$$\hat{\boldsymbol{\beta}}^* \Rightarrow \left[\hat{\boldsymbol{\beta}}_1^*, \hat{\boldsymbol{\beta}}_2^*, \hat{\boldsymbol{\beta}}_3^*\right]$$

where $\hat{\boldsymbol{\beta}}_1^*$ is a 5×5 matrix equal to $[\hat{\boldsymbol{\beta}}_3, \hat{\boldsymbol{\beta}}_4, \hat{\boldsymbol{\beta}}_5, \hat{\boldsymbol{\beta}}_6, \hat{\boldsymbol{\beta}}_7]$ and each element is a 5×1 column vector, $\hat{\boldsymbol{\beta}}_2^*$ is a 4×5 matrix given by $[\hat{\boldsymbol{\beta}}_1, \hat{\boldsymbol{\beta}}_2, \hat{\boldsymbol{\beta}}_{12}, \hat{\boldsymbol{\beta}}_{22}]$ where each element is a 4×1 column vector, and

$\hat{\boldsymbol{\beta}}_3^*$ is a 25×5 matrix of the remaining model coefficients. Substituting into Eq. (A3),

$$\boldsymbol{\delta}\,\hat{\mathbf{y}} = \mathbf{x}_{0_1}^*\hat{\boldsymbol{\beta}}_1^* + \mathbf{x}_{0_2}^*\hat{\boldsymbol{\beta}}_2^* + \mathbf{x}_{0_3}^*\hat{\boldsymbol{\beta}}_3^* \tag{A4}$$

Solving Eq. (A4) for $\mathbf{x}_{0_1}^*$, which contains the primary loads, yields

$$\hat{\mathbf{x}}_{0_1}^* = (\hat{\boldsymbol{\beta}}_1^*)^{-1}[\boldsymbol{\delta}\mathbf{y} - \mathbf{x}_{0_2}^*\hat{\boldsymbol{\beta}}_2^* - \hat{\mathbf{x}}_{0_3}^*\hat{\boldsymbol{\beta}}_3^*] \tag{A5}$$

where $(\hat{\boldsymbol{\beta}}_1^*)^{-1}[\boldsymbol{\delta}\mathbf{y} - \mathbf{x}_{0_2}^*\hat{\boldsymbol{\beta}}_2^*]$ is the uncorrected load, or $\hat{\mathbf{x}}_{0_{\text{uncorrected}}}^*$. The true, corrected load $\hat{\mathbf{x}}_{0_1}^*$ is calculated through iteration since $\hat{\mathbf{x}}_{0_3}^* = f(\hat{\mathbf{x}}_{0_1}^*)$. Initializing the iterative scheme with $\xi = 1$, Eq. (A5) can be expressed as

$$(\hat{\mathbf{x}}_{0_1}^*)_\xi = \hat{\mathbf{x}}_{0_{\text{uncorrected}}}^* - [(\hat{\boldsymbol{\beta}}_1^*)^{-1}\hat{\mathbf{x}}_{0_3}^*\hat{\boldsymbol{\beta}}_3^*]_{\xi-1} \tag{A6}$$

where for the first iteration $[(\hat{\boldsymbol{\beta}}_1^*)^{-1}\hat{\mathbf{x}}_{0_3}^*\hat{\boldsymbol{\beta}}_3^*]_0 = 0$ and $(\hat{\mathbf{x}}_{0_1}^*)_1 = \hat{\mathbf{x}}_{0_{\text{uncorrected}}}^*$. The algorithm is extremely stable because the primary loads dominate, and the iterations continue until convergence of the solution, which is typically within five iterations.

Acknowledgments

This work has been supported and funded by the National Force Measurement Technology Capability (NFMTC), the Aeronautics Test Program (ATP), and the NASA Engineering Safety Center (NESC). The authors would like to express their sincere appreciation to everyone that has contributed to the many aspects of this project. In particular, the authors would like to recognize the following individuals for the critical contributions: Jerald (Greg) Jones for his extensive expertise and knowledge on the single-vector system (SVS) and for his efforts in performing the balance calibration, Ray Rhew for his valuable input on force measurement system design and characterization, Thomas Johnson for updating the data processing code for the SVS, Mark Schoenenberger for his valuable input in determining the calibration requirements in support of his research efforts for the Mars Science Laboratory program, and Matt Rhode for his testing experience and knowledge of previous testing using the SS-12 balance. The authors would like to also acknowledge the reviewers for their suggestions and contributions to the revision of this paper.

References

[1] Dyakonov, A., Schoenenberger, M., Scallion, W., Van Norman, J., Novak, L., and Tang, C., "Aerodynamic Interference Due to MSL Reaction Control System," 41st AIAA Thermophysics Conference, AIAA Paper 2009-3915, San Antonio, TX, June 2009.

[2] Schoenenberger, M., Dyakonov, A., Buning, P., Scallion, W., and Van Norman, J., "Aerodynamic Challenges for the Mars Science Laboratory Entry, Descent and Landing," 41st AIAA Thermophysics Conference, AIAA Paper 2009-3914, San Antonio, TX, June 2009.

[3] Guarino, J., "Calibration and Evaluation of Multi-Component Strain Gage Balances," *NASA Interlaboratory Force Measurements Meeting*, Jet Propulsion Lab., Pasadena, CA, April 1964.

[4] Booth, D., "ABCS Calibration Load Schedule for Force Type Balances," 46th AIAA Aerospace Sciences Meeting and Exhibit, AIAA Paper 2008-844, Reno, NV, Jan. 2008.

[5] Parker, P. A., "A Single-Vector Force Calibration Method Featuring the Modern Design of Experiments," 39th AIAA Aerospace Sciences Meeting and Exhibit, AIAA Paper 2001-170, Reno, NV, Jan. 2001.

[6] *Recommended Practice: Calibration and Use of Internal Strain Gage Balances with Application to Wind Tunnel Testing*, AIAA Standards Series, R-091-2003, AIAA, Reston, VA, 2003.

[7] Box, G. E., and Wilson, K., "On the Experimental Attainment of Optimum Conditions," *Journal of the Royal Statistical Society*, Vol. 13, No. 1, 1951, pp. 1–45.

[8] Myers, R. H., and Montgomery, D. C., *Response Surface Methodology*, 2nd ed., Wiley, New York, 2002.

[9] Montgomery, D., *Design and Analysis of Experiments*, 7th ed., Wiley, New York, 2009.

[10] Fisher, R. A., *Statistical Methods for Research Work*, Oliver and Boyd, Edinburgh, Scotland, U.K., 1925.

[11] Kowalski, S. M., Parker, P. A., and Vining, G. G., "Tutorial on Split-Plot Experiments," *Quality Engineering*, Vol. 19, 2007, pp. 1–15. doi:10.1080/08982110601057179

[12] Parker, P. A., Kowalski, S. M., and Vining, G. G., "Unbalanced and Minimal Point Equivalent Estimation of Second-Order Split-Plot Designs," *Journal of Quality Technology*, Vol. 39, 2007, pp. 376–388.

[13] Parker, P. A., Anderson-Cook, C. M., Robinson, T., and Liang, L., "Robust Split-Plot Designs," *Quality and Reliability Engineering International*, Vol. 24, 2008, pp. 107–121. doi:10.1002/qre.886

[14] Corbeil, R., and Searle, S., "A Comparison of Variance Component Estimators," *Biometrics*, Vol. 32, No. 4, Dec. 1976, pp. 779–791. doi:10.2307/2529264

[15] Milliken, G. A., and Johnson, D. E., *Analysis of Messy Data*, Vol. 1, Designed Experiments, Lifetime Learning, Belmont, CA, 1984.

[16] Myers, R. H., *Classical and Modern Regression with Applications*, 2nd ed., Duxbury, Belmont, CA, 1990.

[17] Bergman, R., and Philipsen, I., "An Experimental Comparison of Different Load Tables for Balance Calibration," *7th International Symposium on Strain Gage Balances*, April 2010.

[18] Ulbrich, N., "Regression Model Optimization for the Analysis of Experimental Data," 47th AIAA Aerospace Sciences Meeting and Aerospace Exposition, AIAA, Paper 2009-1344, Orlando, FL, Jan. 2009.

[19] Montgomery, D., Peck, E., and Vining, G. G., *Introduction to Linear Regression Analysis*, 4th ed., Wiley, New York, 2006.

[20] Moore, T., "Recommended Strain Gage Application Procedures for Various Langley Research Center Balance and Test Articles," NASA, TM-2004-213017, May 2004.